Rotational modulation in *TESS* B stars

L. A. Balona [1]★ G. Handler,[2] S. Chowdhury,[2] D. Ozuyar,[3] C. A. Engelbrecht,[4]
G. M. Mirouh,[5] G. A. Wade,[6] A. David-Uraz [7] and M. Cantiello[8,9]

[1]*South African Astronomical Observatory, PO Box 9, Observatory, Cape Town 4735, South Africa*
[2]*Nicolaus Copernicus Astronomical Center, Bartycka 18, PL-00-716 Warsaw, Poland*
[3]*Department of Astronomy and Space Science, Ankara University, 06100 Tandogan, Ankara, Turkey*
[4]*Department of Physics, University of Johannesburg, PO Box 524, Auckland Park, Johannesburg 2092, South Africa*
[5]*Astrophysics Research Group, Faculty of Engineering and Physical Sciences, University of Surrey, Guildford GU2 7XH, UK*
[6]*Department of Physics & Space Science, Royal Military College of Canada, PO Box 17000, Station Forces, Kingston, ON K7K 7B4, Canada*
[7]*Department of Physics and Astronomy, University of Delaware, Newark, DE 19716, USA*
[8]*Center for Computational Astrophysics, Flatiron Institute, 162 5th Avenue, New York, NY 10010, USA*
[9]*Department of Astrophysical Sciences, Princeton University, Princeton, NJ 08544, USA*

ABSTRACT

Light curves and periodograms of 160 B stars observed by the Transiting Exoplanet Survey Satellite (*TESS*) space mission and 29 main-sequence B stars from *Kepler* and *K2* were used to classify the variability type. There are 114 main-sequence B stars in the *TESS* sample, of which 45 are classified as possible rotational variables. This confirms previous findings that a large fraction (about 40 per cent) of A and B stars may exhibit rotational modulation. *Gaia* DR2 parallaxes were used to estimate luminosities, from which the radii and equatorial rotational velocities can be deduced. It is shown that observed values of the projected rotational velocities are lower than the estimated equatorial velocities for nearly all the stars, as they should be if rotation is the cause of the light variation. We conclude that a large fraction of main-sequence B stars appear to contain surface features which cannot likely be attributed to abundance patches.

Key words: stars: early-type – stars: oscillations – stars: rotation.

1 INTRODUCTION

The existence of large spots or spot groups on the surfaces of cool stars other than the Sun is well established. This discovery can be traced back to Kron (1947) who observed four eclipsing binaries and detected significant light variability outside eclipse that could not be explained other than by the presence of spots similar to those on the Sun. These stars were later called RS CVn binaries. Hall (1972) was the first to explicitly postulate the starspot model in these stars. Rotational modulation due to starspots is also detected in the BY Dra variables, which are emission-line K and M dwarfs, and in the FK Com stars, which are rapidly rotating G–K giants with emission in the CaII lines. Over 500 field stars showing evidence of starspots are known (see Strassmeier 2009 for a review), but many thousands have been detected from the *Kepler* space mission (McQuillan, Mazeh & Aigrain 2013, 2014; Nielsen et al. 2013; Reinhold, Reiners & Basri 2013; Chowdhury et al. 2018).

Sunspots appear cooler than the surrounding photosphere because they correspond to regions of lower convective energy transport. The decrease in energy transport is due to strong localized magnetic fields which affect the convective motions close to the stellar surface. The magnetic fields are thought to be a result of dynamo action in the convective outer envelope of the Sun and other cool stars (Charbonneau 2014). From this perspective, only stars with outer convective envelopes can support such a magnetic field. Hence dark starspots are not expected in A and B stars which have radiative envelopes.

The chemically peculiar Ap and Bp stars do, however, show rotational light modulation due to patches of differing chemical abundances on the stellar surface. The chemical peculiarities are believed to be confined to the outer layers of the star and are generally thought to be a result of gravitational settling and diffusion of elements in the presence of a strong global magnetic field (Michaud 1970). For these stars, which have radiative atmospheres, the magnetic field is thought to be of fossil origin.

The discovery that a large fraction of A and B stars observed by *Kepler* seem to show rotational modulation (Balona 2013, 2016, 2017) and some of them possibly even flares (Balona 2012) was therefore unexpected. The possible existence of rotational modulation among the B stars suggests that our current understanding of the physics of the outer layers of hot stars may need to be revised. The fact that a great majority of δ Scuti stars show unexpected low

---

★ E-mail: lab@saao.ac.za

frequencies (Balona 2018), which cannot be explained by current models, also points to such a revision.

The Transiting Exoplanet Survey Satellite mission (*TESS*; Ricker et al. 2015) is designed to search for exoplanets. A preliminary report on B stars from the first set of observations (Sectors 1 and 2) covering 55 d can be found in Pedersen et al. (2019). Our main aim is to classify the *TESS* B stars observed in Sectors 1 and 2 into various variability types, to estimate the approximate fraction of main-sequence stars which might be rotational variables and to determine if the photometric periods are consistent with the presumed rotational periods.

2 DATA AND ANALYSIS

TESS observes the sky in sectors measuring $24° \times 96°$ that extend from near the ecliptic equator to beyond the ecliptic pole. Each sector is observed for two orbits of the satellite around the Earth, or about 27 d. Sectors begin to overlap towards the ecliptic pole which means that at mid-latitudes the same star will be observed in more than one sector. There is a continuous viewing zone near the ecliptic pole where the same stars are observed in all sectors.

The data analysed in this paper are from the light curves of the first release (Sectors 1 and 2). Most of the stars discussed here are at mid-latitudes and have been observed for a time span of about 55 d. A description of how these data products were generated is found in Jenkins et al. (2016).

Light curves are generated with two-minute cadence using simple aperture photometry (SAP) and pre-search data conditioning (PDC). The PDC pipeline module uses singular value decomposition to identify and correct for time-correlated instrumental signatures in the light curves. In addition, PDC corrects the flux for each target to account for crowding from other stars and their effects. Only PDC light curves are used in this paper.

The noise level in the amplitude periodogram is around 10 ppm for the brightest stars, about 30 ppm at about $V = 8$ mag, 100 ppm at $V = 10$ mag, and 200 ppm at $V = 12$ mag. A frequency peak with a false alarm probability of 10^{-3} or less is taken as being significant.

The *TESS* input catalogue (Stassun et al. 2018) lists stellar parameters for stars observed by *TESS*. The effective temperatures, T_{eff}, for stars without spectroscopic determinations were obtained from near-infrared photometry, which is not reliable for B stars, particularly since reddening is important in many cases. The stars observed by *TESS* were matched with the SIMBAD astronomical data base (Wenger et al. 2000) and only those known to be B stars were selected, giving a total of 160 stars with spectral types earlier than A0.

Periodograms and light curves were visually inspected and each star assigned a variability class where appropriate. A necessary signature of rotational modulation is taken to be a significant, isolated low-amplitude peak with frequency less than $4 \, \text{d}^{-1}$ or a low-amplitude peak with one or more harmonics. The classification was made independently by LAB and GH with agreement among the stars deemed to be rotational variables.

3 ROTATIONAL VARIABILITY

The equatorial rotational velocity, v_e (km s^{-1}), is given by $v_e = 50.74 \nu_{rot}(R/R_\odot)$, where the rotational frequency, ν_{rot} is in cycles d^{-1} and $R/R_\odot$ is the stellar radius in solar units. For main-sequence B stars the radii are typically 2–10 R/R$_\odot$ and v_e in the range 0–400 km s^{-1}. Thus one might expect $0 < \nu_{rot} < 4 \, \text{d}^{-1}$.

A periodogram peak in this frequency range could be a result of rotational modulation.

There are two ways to show that the variability of a group of stars might be due to rotational modulation. One way is to demonstrate that there is a relationship between the projected rotational velocities, $v \sin i$, and the equatorial rotational velocities, v_e. Since $\sin i \leq 1$, the expectation is that in a plot of $v \sin i$ as a function of v_e, the points will all lie on or below the line $v \sin i = v_e$, subject to measurement errors (see figure 2 in Balona 2017).

Another method is to show that, for stars in the main-sequence band, the distribution of v_e, derived from ν_{rot} and an estimate of the stellar radii, matches the distribution of v_e derived from spectroscopic measurements of $v \sin i$ for stars in the general field within the same temperature range (see figure 8 in Balona 2013). This has the advantage that values of $v \sin i$ of the stars to be tested are not required. A sufficient number of stars in each v_e bin is necessary and the number of bins needs to be sufficiently large to adequately resolve the distribution. The method therefore requires a rather large number of stars. The number of B stars with photometrically derived rotation periods is, at present, too few for this method to be applied.

Classification of stars according to variability type is an essential first step in any analysis. The information at hand is very limited: the light curve, the periodogram, and the approximate location of the star in the H–R diagram as judged by the spectral type and the *Gaia* DR2 parallax.

It is reasonable to adopt the variability type definitions in the *General Catalogue of Variable Stars* (GCVS; Samus, Durlevich & et al. 2009). There may be variability which does not seem to fit in any of the GCVS classes. Unless there is additional supporting evidence, the temptation must be resisted to assign a new class of variable. Since the GCVS does not include a type for rotational variables among the A and B stars, we have chosen ROT as a suitable designation for any star exhibiting rotational modulation, but not known to be chemically peculiar.

The SXARI variables are a specific set of B0p–B9p rotational variables with variable-intensity He I and Si III lines and magnetic fields. The periods of their light and magnetic field variations are consistent with rotation. They are high-temperature analogues of the α^2 CVn (ACV) variables, which are Ap stars with a tilted global magnetic field and abundance patches, giving rise to rotational modulation of the light curve. If a star shows signs of abnormalities, such as enhanced Si, Mg, or Hg or is He weak or He strong, then the variability is likely a result of a patch or patches of enhanced chemical abundance. For the purpose of this study, we classify these stars as SXARI rather than ACV or ROT so as to distinguish between two different causes of rotational modulation: localized abundance anomalies or localized temperature differences. The photometric frequency in both cases is the rotational frequency.

Binaries in a circular orbit may give rise to a low frequency peak either through tidal effects (ELL type of variable) or grazing eclipses. Eclipses are easy to spot as they give rise to a large number of harmonics in the periodogram. Tidal effects cannot easily be distinguished from rotational modulation. The ambiguity between the ELL and ROT classifications can be broken if there is significant amplitude or frequency modulation.

4 OTHER TYPES OF VARIABILITY IN B STARS

There are two main types of pulsating variable among the B stars, the β Cep (called BCEP in the GCVS) and 'slowly pulsating B-star' (SPB) variables. The pulsations in both types are caused by the

opacity mechanism in the ionization zone of iron-group elements (Dziembowski, Moskalik & Pamyatnykh 1993). The β Cep stars are hotter (20 000–32 000 K) and pulsate with frequencies in the range 4–12 d^{-1}, while the SPB stars are cooler (11 000–19 000 K) and pulsate with frequencies in the range 0.3–3 d^{-1}.

In the GCVS, SPB stars are given the variability type LPB ('long-period B-star'). The reason for the different designation is that the GCVS wisely tries to avoid naming a variable type according to a specific interpretation of the cause of the light variation. If a much better interpretation for SPB light variations were to be found, for example, then the class will have to be renamed. However, since the designation LPB has fallen into disuse, SPB is used instead.

The ACYG variables are non-radially pulsating B-type super-giants. The multiple periods range from several days to several weeks. The B supergiants observed by *TESS* are all members of the Large Magellanic Cloud (LMC). With few exceptions, the light curves of all the LMC supergiants matched those expected for the ACYG variables.

The Be variables are B stars which show, or have shown, emission in Hα or other Balmer lines. This can include many different types of object, including supergiants, in which the emission is thought to be due to different physical mechanisms. The 'classical Be stars' are a narrower set confined to stars in the main-sequence band. Some Be stars show large, frequent outbursts in the light curve attributed to the sudden ejection of circumstellar material (GCAS variables). Others are less active and show quasi-periodic variations with time-scales in the range 0.5–2 d, usually attributed to multiple non-radial pulsations and/or obscuration by circumstellar material. In the GCVS, the designation BE is used to describe these stars. The photometric variability type BE should not be confused with the spectroscopic classification 'Be' which designates emission in some Balmer lines.

The EA and EB variables are eclipsing binaries. In EA variables it is possible to specify the beginning and end of eclipses. Between eclipses the light is more-or-less constant. On the other hand, the EB eclipsing variables are close binaries where the variation is practically sinusoidal with no constant light. The EP stars show very small eclipses which may be attributed to a planet or sub-stellar companion.

The MAIA type is a new class which was introduced by Balona et al. (2015, 2016). These are B stars which show many high-frequency peaks similar to those seen in BCEP or δ Scuti variables (called DSCT in the GCVS). However, they are too cool to be classified as BCEP and too hot to be DSCT. Whether or not they deserve a separate class remains to be seen. These stars may be related to the 'FaRPB' stars (Mowlavi et al. 2016) which also show high frequencies and lie between the β Cep and δ Scuti variables. The FaRPB stars, however, are all rapidly rotating stars. The evidence suggests that MAIA stars are not rapid rotating stars (Balona et al. 2016).

Some subdwarf B stars (sdB stars) are also known to be multiperiodic variables. There are two classes: the V361 Hya and the V1093 Her stars. V361 Hya stars are short-period pulsating sdB stars with $24\,000 < T_{\rm eff} < 40\,000$ K and $\log g < 5.8$ (less compact than white dwarfs). They have multiple periods in the range 60–400 s (200–1500 d^{-1}). They are also known as EC 14026 stars. The V1093 Her stars are in the same general area of the H–R diagram, but somewhat cooler and less compact. They are long-period (1800–9000 s or 10–50 d^{-1}) analogues of the V361 Hya stars and are also known as PG 1716 stars.

Table 1 lists our assigned variability type in the third column. Where the star seems constant or no definite assignment is possible,

a dash is used. When the classification is uncertain a question mark is added (e.g. ROT?). Sometimes two classifications are possible and either is acceptable. This is shown by a slash, e.g: ROT/ELL. In other cases two types seem to be present in the same star which is shown by a plus, e.g. SPB + ROT. The classification of ROT in a pulsating star such as SPB or BCEP is sometimes made if a strong peak and its harmonic are present. The justification is that there is no reason why rotational modulation cannot co-exist with pulsation. The harmonic may, of course, also arise as a result of non-linear pulsation. Fig. 1 shows some examples of the periodograms and the phased light curves of stars classified as a ROT variables.

5 EFFECTIVE TEMPERATURE

The effective temperature, $T_{\rm eff}$, may be estimated in several different ways, sometimes giving very different results. Literature values of $T_{\rm eff}$ were chosen according to the following order of descending priority.

Whenever possible, estimates of $T_{\rm eff}$ from modelling the stellar spectrum were chosen. Failing this, an estimate based on narrow-band photometry (i.e. Strömgren *uvbyβ* or Geneva photometry) was used For some stars, Strömgren photometry was available, but no value of $T_{\rm eff}$ had yet been derived. In such cases we estimated $T_{\rm eff}$ by de-reddening the star using the method described by Crawford (1978) and then applying the calibrations of Balona (1994) to obtain $T_{\rm eff}$.

Next in priority were methods using the spectral energy distribution (SED) from wide-band photometry, usually UBVRI. There can be problems with this method if measurements in the U band are missing, so $T_{\rm eff}$ from SED was selected only if it agreed reasonably well with the temperature from the spectral type. If not, or if no $T_{\rm eff}$ measurements could be found, the spectral type itself was used to estimate $T_{\rm eff}$ from the table of Pecaut & Mamajek (2013). For emission-line stars the $T_{\rm eff}$ from the spectral type was used instead of photometric methods.

The error in $T_{\rm eff}$ clearly depends on the method used, but we can obtain an approximate overall value for B stars from the PASTEL catalogue (Soubiran et al. 2016). The errors increase with $T_{\rm eff}$ ranging from 500 to 1500 K. We adopt a standard error of 1000 K as reasonable overall estimate.

6 LUMINOSITIES AND RADII

From the *Gaia* DR2 parallax π (Gaia Collaboration 2016, 2018), the absolute magnitude is calculated using $M_V = V_0 + 5(\log_{10}\pi + 1)$, where V_0 is the reddening-free V magnitude. We used V magnitudes from SIMBAD. The reddening correction was derived from a three-dimensional reddening map with a radius of 1200 pc around the Sun and within 600 pc of the galactic mid-plane as calculated by Gontcharov (2017). For more distant stars, a simple reddening model is used (see equation 20 of Brown et al. 2011), but adjusted so that it agrees with the 3D map at 1200 pc.

The absolute bolometric magnitude is given by $M_{\rm bol} = M_V + {\rm BC}_V - M_{\rm bol\odot}$, where ${\rm BC}_V$ is the bolometric correction in V and $M_{\rm bol\odot} = 4.74$ is the absolute bolometric magnitude of the Sun. The bolometric correction as a function of $T_{\rm eff}$ is given in Pecaut & Mamajek (2013). Finally, the luminosity relative to the Sun is found using $\log L/{\rm L}_\odot = -0.4 M_{\rm bol}$. *Gaia* DR2 parallaxes for many early-type stars are subject to larger errors than quoted because the match with the astrometric model used to determine the parallax is rather poor, perhaps due to binarity (Gaia Collaboration et al. 2018). Nevertheless, these are the best parallax estimates at present. From

Table 1. List of B stars observed by *TESS*. The TIC number and the star name are given in the first two columns. This is followed by the assigned variability type (GCVS type in brackets) and the apparent *V* magnitude. The presumed rotational frequency, ν_{rot}, the amplitude, A_{rot}, the signal-to-noise ratio, S/N, of the periodogram peak, and the number of visible harmonics, N_H, is *shown*. The derived equatorial rotational velocity is v_e and $v\sin i$ is the projected rotational velocity from the literature. The adopted effective temperature is T_{eff} as derived from the reference (see Table 2). Finally, the stellar luminosity obtained from the *Gaia* parallax and the spectral type are shown ['(Be)' indicates a classical Be star].

TIC	Name	Var. type	V (mag)	ν_{rot} (d^{-1})	A_{rot} (ppm)	S/N	N_H	v_e (km s^{-1})	$v\sin i$ (km s^{-1})	T_{eff} (K)	Ref	$\log\frac{L}{L_\odot}$	Sp. type
12359289	HD 225119	SXARI	8.180	0.325	4157	95	1	65		15 330	1	2.90	kB8hB7HeB9.5IIISi
29990592	HD 268623	ACYG	11.635							20 665	2		B1.5Ia (LMC)
30110048	HD 268653	ACYG	10.760							17 185	2		B2.5Ia (LMC)
30268695	HD 268809	ACYG	11.964							22 845	2		B0.5Ia (LMC)
30275662	Sk-66 27	ACYG	11.779							17 765	2		B2.5/3Ia (LMC)
30312676	HD 268726	ACYG	11.265							19 075	2		B2Iaq (LMC)
30317301	HD 268798	EB	11.490							28 000	1		B0.5, B2Ia (LMC)
30933383	Sk-68 39	ACYG	12.039							22 580	1		B2.5Ia (LMC)
31105740	TYC 9161-925-1	ACYG	12.010							24 970	2		B0.5Iae (LMC)
31181554	HD 269050	ACYG	11.540							25 000	1		B0Ia(e?) (LMC)
31674330	GJ 127.1	–	11.394						0	16 860	3	−2.75	DA3.0
31867144	HD 22252	SPB	5.806						223	12 157	4	2.72	B8IV
33945685	HD 223118	ROT	8.250	2.835	72	25	0	273		10 500	5	1.60	B9V
38602305	HD 27657	ROT	5.870	0.336	920	143	3	42		12 448	7	2.13	B9III/IV; A2–A7 m
40343782	HD 269101	ACYG?	12.030							21 370	1		B3Iab; (LMC)
41331819	HD 43107	ROT	5.044	0.714	324	91	0	106	98	10 886	4	2.04	B9.5III, B8V
47296054	HD 214748	SPB + ROT	4.180	0.836	63	51	3	202	180	13 520	1	2.84	B8IVe (Be)
49687057	HD 220787	–	8.290						26	17 379	6	3.54	B3III
53992511	HD 209522	BE (BE)	5.952						280	22 570	1	3.51	B4IVe (Be)
55295028	HD 33599	BE	8.970						200	22 570	1	4.44	B3p shell: (Be)
66497441	HD 222847	ELL	5.235						307	12 000	8	2.24	B8.5Vnn
69925250	V* HN Aqr	BCEP + SPB (BCEP)	11.470						45	22 909	8	4.31	B0/1
89545031	HD 223640	SXARI (ACV)	5.180	0.266	9000	95	1	36	27	12 462	9	2.20	B9SiSrCr*
92136299	HD 222661	ROT + FLARE?	4.483	2.251	217	82	1	225	120	11 108	8	1.73	B9.5IV
115177591	HD 201108	ROT	6.900	1.736	2442	89	0	345		10 158	10	2.17	B8IV/V
118327563	CD-38 222	ROT + FLARE?	10.260	4.372	733	60	1	54	48	26 300	11	1.42	sdB
139468902	HD 213155	ROT	6.924	2.199	288	87	1	264		9628	6	1.64	B9.5V
141281495	HD 37854	ROT	8.100	0.334	205	89	0	48		10 500	5	1.96	B9/9.5V
147283842	HD 205805	–	10.180							25 000	11	1.67	sdB4
149039372	HD 34543	SPB?	8.370							11 583	6	2.12	B8V
149971754	HD 41297	SPB	10.000							13 520	7	2.57	B8IV
150357404	HD 45796	SPB + ROT?	6.248	0.640	10 333	77	0	114	17	13 775	6	2.61	B6V
150442264	HD 46792	EB (EB:)	6.140							16 605	6	3.42	B3(V)k
152283270	HD 208433	EA + ROT?	7.440	0.434	80	26	0	69		10 500	5	2.04	B9.5V
167045028	HD 45527	EB?	9.910	0.329	5811	135	1	62		11 000	1	2.27	B9IV
167415960	HD 48467	–	8.270							10 613	7	2.19	B8/9V
167523976	HD 49193	SPB	8.940							24 380	1	4.06	B2V
169285097	CD-35 15910	sdB hybrid	11.000							28 390	11	1.50	sdB He1
176935619	HD 49306	ROT	6.700	2.748	29	26	0	326		10 082	7	1.71	B9.5/A0V
176955379	HD 49531	ROT	8.910	2.994	1181	109	1	414		11 900	5	2.13	B8/9Vn
177075997	HD 51557	ROT?	5.393	0.352	49	44	0	89	124	12 325	6	2.72	B7III
179308923	HD 269382	ACYG + EB?	10.815							27 600	1		O9.5Ib (LMC)
179574710	HD 271213	ACYG	12.310							23 790	1		B1Iak (LMC)
179637387	[OM95]LH47-373A	ACYG?	11.970							20 300	12		B1Ib (LMC)
179639066	HD 269440	ACYG	11.378							22 240	2		B1.5Ia (LMC)
181043970	HD 5148	EA (EA/SD)	10.640							11 000	5	1.41	B9/A2IV:
182909257	HD 6783	SXARI	7.940	0.319	2837	92	3	36	30	12 941	6	2.11	B8Si
197641601	HD 207971	ROT?	3.010	0.201	135	36	0	68	55	11 984	6	2.92	B8IV-Vs
206362352	HD 223145	SPB	5.161						240	17 163	4	3.03	B2.5V
206547467	HD 210780	ROT	8.340	0.233	75	25	1	16		12 500	7	1.61	B9.5/A0V
207176480	HD 19818	BE	9.060							11 710	5	1.59	B9/A0Vne: (Be)
207235278	HD 20784	ELL	8.280	0.558	4530	95	1	187		9175	7	2.45	B9.5V
220430912	HD 31407	EA (EA)	7.690							19 648	7	3.76	B2/3V
224244458	HD 221507	SXARI + FLARE	4.370	0.522	141	80	2	57	21	12 380	6	2.00	B9.5IVpHg:Mn:Eu:
229013861	HD 208674	ROT?	7.920	0.423	80	23	0	35		14 555	7	2.04	B9.5V
230981971	HD 10144	BE (BE)	0.460						225	20 760	1		B4V(e) (Be)
231122278	HD 29994	SPB	8.110							11 900	5	2.08	B8/9V
238194921	HD 24579	SPB + ROT	8.060	0.727	74	37	0	114		15 330	1	2.68	B7III
259862349	HD 16978	ROT?	4.106	0.402	51	31	0	53	96	10 003	6	1.79	B9V
260128701	HD 42918	SPB	7.950							16 289	7	3.00	B4V

Table 1 *– continued*

TIC	Name	Var. type	V (mag)	ν_{rot} (d^{-1})	A_{rot} (ppm)	S/N	N_H	v_e (km s^{-1})	$v\sin i$ (km s^{-1})	T_{eff} (K)	Ref	$\log \frac{L}{L_\odot}$	Sp. type
260131665	HD 42933	EB (EB/D:)	4.810						170	25 981	6	4.58	B0.5:III?np + B0.5/3:
260368525	HD 44937	ROT?	8.190	1.194	31	16	1	241		10 500	5	2.24	B9.5V
260540898	HD 46212	ROT?	8.260	0.562	30	11	1	117		12 400	5	2.56	B8IV
260640910	HD 46860	BE	5.707						200	13 520	1	2.70	B8III (Be)
260820871	HD 218801	EP	8.990							10 500	5	1.92	B9.5Vn:
261205462	HD 40953	SPB	5.451						23	11 243	4	1.93	B9V
262815962	HD 218976	ROT	8.120	0.369	207	58	1	40		9846	6	1.60	B9.5/A0V
270070443	HD 198174	SXARI	5.854	0.395	2529	99	0	64	72	13 217	13	2.46	B7IIIp
270219259	HD 209014	BE + MAIA	5.620						350	13 520	1	2.96	B8III shell (Be)
270557257	HD 49835	ROT?	8.560	2.475	42	13	0	253		10 500	5	1.65	B9.5V
270622440	HD 224112	–	6.828						35			2.32	Blend with 270622446
270622446	HD 224113	EA (EA/DM)	6.087						135	13 665	4	2.70	B7(V) + B9(V)
271503441	HD 2884	ROT	4.335	3.056	234	51	1	282	140	11 576	14	1.73	B8/A0
271971626	HD 62153	ROT + MAIA	7.020	0.215	289	88	0	38		11 783	4	2.33	B9IV
276864600	HD 269777	ACYG	11.060							21 370	1		B3Ia (LMC)
277022505	HD 269786	ACYG	11.180							28 000	1		B1I (LMC)
277022967	HD 37836	ACYG	10.660							28 000	1		B0e(q)I (LMC)
277099925	HD 269845	ACYG	11.790							22 580	1		B2.5Ia (LMC)
277103567	HD 37935	ROT (BE)	6.281	1.496	209	74	3	361	209	9940	6	2.30	B9.5V (Be)
277172980	HD 37974	ACYG	10.959							28 000	1		B0.5e (LMC)
277173650	HD 269859	ACYG	10.730							23 790	1		B1.5Ia (LMC)
277298891	Sk-69 237	ACYG	12.080							24 625	2		B1Ia (LMC)
277982164	HD 54239	ROT	5.459	1.266	122	66	1	248	209	9938	4	2.12	B9.5/A0III/IV
278683664	HD 47770	ROT?	8.490	1.701	32	13	0	268		9012	7	1.76	B9.5V
278865766	HD 48971	–	8.280							9743	7	1.93	B9V
278867172	HD 49111	–	8.490							14 273	7	2.11	B9.5V
279430029	HD 53048	ROT	7.920	1.784	64	33	1	554		18 950	1	3.64	B5/7Vn(e:) (Be)
279511712	HD 53921	ELL (LPB)	5.600	0.605	4590	141	1	141		13 800	4	2.84	B9III + B8V
279957111	HD 269582	–	12.597							30 200	1		Ofpe/WN9 (LMC)
280051467	HD 19400	SXARI	5.497	0.229	570	135	0	36	64	14 117	6	2.56	B8III/IV Hewk
280684074	HD 215573	SPB + ROT (LPB)	5.313	0.563	10 068	77	0	104	13	13 960	15	2.66	B6V
281703963	HD 4150	MAIA	4.365						105	9822	14	2.06	A0IV/B9Vp((SiFe))
281741629	CD-56 152	BE (BE)	10.180						180	19 000	16	4.59	sdB?/Be?
293268667	HD 47478	SPB + ROT	8.500	3.390	386	75	1	455		10 765	7	1.93	B9V
293271581	Hen 3-15	EB (NB)	12.502									0.67	Bem RR Pic (Nova)
293973218	HD 54967	SPB	6.470						34	22 570	1	3.47	B3III
294747615	HD 30612	SXARI	5.515	0.192	670	130	0	30	30	13 661	6	2.50	B8II/IIIp:Si:
294872353	HD 270754	ACYG	11.260							19 910	2		B1.5Ia: (LMC)
300010961	HD 55478	ROT + MAIA	8.060	0.683	723	117	3	122		11 144	7	2.24	B8III
300325379	HD 58916	ROT	8.010	1.838	42	20	0	268		11 710	1	2.15	B9Vn
300329728	HD 59426	ELL/ROT	8.420	0.411	5216	140	1	51		11 710	1	2.02	B9V
300744369	HD 63928	ROT	8.700	0.957	475	115	1	102		11 710	1	1.88	B9V
300865934	HD 64484	–	5.774							10 707	4	2.14	B9V
306672432	HD 67252	ROT?	8.530	1.090	31	13	1	119		13 520	1	2.15	B8/9V
306824672	HD 68221	SPB?	8.650							11 710	5	2.32	B9V
306829961	HD 68520	SPB	4.400						10	14 090	17	3.44	B5III
307291308	HD 71066	SXARI	5.617	0.387	300	42	1	62	2	11 821	6	2.25	B9pMnHg
307291318	HD 71046	–	5.329						69	12 102	6	2.37	B9III/IV
307993483	HD 73990	SPB + ROT?	6.870	3.697	48	27	0			10 221	7	2.02	B7/8V
308395911	HD 66591	SPB	4.797						43	16 983	6	2.96	B3IV
308454245	HD 67420	MAIA	8.250							11 710	1	2.15	B9V
308456810	HD 67170	ROT	8.110	0.251	54	23	1	38		13 520	1	2.43	B8III/IV
308537791	HD 67277	ROT + MAIA	8.260	0.527	746	81	1	78		13 520	1	2.41	B8III
308748912	HD 68423	–	6.313							15 330	1	2.86	B7IVek (Be)
309702035	HD 271163	ACYG	9.984							21 370	1		B3Ia (LMC)
313934087	HD 224990	SPB	5.023						15	16 100	17	3.08	B4III
327856894	HD 225253	–	5.581							13 123	6	2.64	B8IV/V
349829477	HD 61267	–	8.330							10 000	1	1.72	B9/A0IV
349907707	HD 61644	EA (EA)	8.410							18 000	1	2.76	B5/6IV
350146577	HD 63204	SXARI	8.310	0.544	48 570	139	1	78		10 505	10	1.95	B9Si
350823719	HD 41037	EB	9.460						215	22 570	3	3.70	B3V
354671857	HD 14228	ROT?	3.570	2.908	256	98	0	375	200	12 687	6	2.18	B8IV-V
355141264	HD 208495	–	8.860							9945	7	1.58	B9.5V
355477670	HD 220802	ROT?	6.210	0.272	21	23	0	37	123	11 206	4	2.03	B9V

Table 1 – *continued*

TIC	Name	Var. type	V (mag)	ν_{rot} (d^{-1})	A_{rot} (ppm)	S/N	N_H	ν_e (km s^{-1})	$\nu\sin i$ (km s^{-1})	T_{eff} (K)	Ref	$\log\frac{L}{L_\odot}$	Sp. type
355653322	HD 224686	ROT	4.470	1.266	117	38	1	274	275	11 710	1	2.49	B9IIIn (Be)
358232450	HD 6882	EA (EA/DM)	3.967						111	13 471	6	2.41	B6V + B9V
358466708	CD-60 1931	ROT	8.090	1.661	3405	83	1	280	223	12 814	18	2.43	B8III
358467049	CPD-60 944	SXARI	8.756	0.265	13 161	97	0	30		12 600	18	2.07	B8pSi
358467087	CD-60 1929	SPB?	8.520						43	12 543	18	2.26	B8.5IV
364323837	HD 40031	SPB?	9.270						65	14 000	16	3.08	sdB, B6III
364398190	CD-60 1978	ROT	8.750	0.760	129	28	0	101	68	12 337	18	2.16	B8.5IV-V
364398342	HD 66194	BE (GCAS)	5.810						200	20 632	18	3.76	B2IVn(e)p(Si) (Be)
364421326	HD 66109	ROT?	8.190	1.976	31	11	0	385		11 710	1	2.40	B9.5V
369397090	CD-30 19716	–	12.860							39 811	19	1.43	sdB
369457005	HD 197630	SPB?	5.474							11 511	6	1.99	B8/9V
370038084	HD 26109	–	8.580							11 710	1	1.62	B9.5/A0V
372913233	HD 65950	–	6.870						26	12 842	18	2.88	B8.5IIIpMnHg
372913582	CD-60 1954	SPB?	8.590						188	10 579	18	2.13	B9.5V
372913684	HD 65987	SXARI (EA:)	7.590	0.685	5892	93	2	163	13	12 600	18	2.70	B9.5IVpSi
373843852	HD 269525	ACYG	12.780							28 000	1		B0: (LMC)
389921913	HD 270196	ACYG	11.600							22 875	2		B1.5Ia (LMC)
391810734	HD 269655	ACYG	12.200							28 800	20		B0Ia (LMC)
391887875	HD 269660	ACYG	11.190							23 790	1		B1.5Ia (LMC)
404768847	VFTS 533	ACYG?	11.820						57	19 275	2		B1.5Ia + qp (LMC)
404768956	NGC 2070 Mel 12	ACYG?	11.996							28 510	20		B0/0.5Ia (LMC)
404796860	HD 269920	ACYG	11.650							18 950	1		B5Ia (LMC)
404852071	Sk-69 265	ACYG	11.880							21 370	1		B3Ia (LMC)
404933493	HD 269997	ACYG	11.200							22 580	1		B2.5Ia (LMC)
404967301	HD 269992	ACYG	11.220							18 020	2		B2.5:Ia: (LMC)
410447919	HD 64811	ROT?	8.450	0.219	317	58	0	133		20 760	1	4.38	B4III
410451677	HD 66409	SXARI	8.410	0.488	1292	98	0	67	34	12 987	18	2.28	B8.5IV(HgMn)?
419065817	HD 1256	ROT	6.488	1.474	138	52	3	186	166	14 280	6	2.37	B6III/IV
425057879	HD 269676	EB/ELL?	11.550						120	41 000	1		O6 + O9 (LMC)
425064757	HD 269696	EA (EA/D)	11.138							42 000	19		sdO (LMC)
425081475	HD 269700	ACYG	10.540							23 790	1		B1.5Iaeq (LMC)
425083410	HD 269698	ACYG	12.220							40 400	1		O4If (LMC)
425084841	TYC 8891-3638-1	ACYG	12.180						62	23 660	2		B1Ia (LMC)
441182258	HD 210934	SPB + ROT?	5.430	1.274	66	26	0	235	56	12 526	6	2.47	B8III
441196602	HD 211993	ROT?	8.200	0.144	49	15	0	20		10 750	6	1.96	B8/9V
469906369	HD 212581	MAIA	4.495						200	11 271	8	2.18	B9.5IVn

the error in the *Gaia* DR2 parallax, the typical standard deviation in $\log(L/L_\odot)$ is estimated to be about 0.05 dex, allowing for standard deviations of 0.01 mag in the apparent magnitude, 0.10 mag in visual extinction and 0.02 mag in the bolometric correction in addition to the parallax error. The true error in luminosity is likely larger for the reason just quoted.

From the luminosity and effective temperature, the stellar radius, $R/R_\odot$, can be found. For stars where the rotational modulation frequency ν_{rot} is available, the equatorial rotational velocity ν_e can be determined. Table 1 shows $\log L/L_\odot$. For those stars with known ν_{rot}, ν_e is also shown.

In addition to the *TESS* stars, we have examined the light curves of *Kepler* and *K2* data for possible rotational modulation. The *Kepler* data have a time span of nearly 4 yr which results in a very low periodogram noise level. The *K2* data have a time span of around 80 d. Table 3 lists the measurements and stellar parameters obtained in the same way. Fig. 2 shows the main-sequence stars in Tables 1 and 3 in the theoretical H–R diagram.

7 ROTATIONAL MODULATION

Since there is evidence that rotational modulation is present in nearly half of the *Kepler* A stars (Balona 2013, 2017), it is reasonable to

presume that rotational modulation may also be common among B stars. The physics of the outer layers of these stars are very similar and we expect continuity in the properties of early A stars and late B stars.

Low frequencies similar to those expected from rotational modulation can also be found in mid- to late-B stars. These are the SPB variables which pulsate with multiple frequencies in the range 0.3–3.0 d^{-1}. For a late B star with ν_e =50–100 km s^{-1}, we expect $\nu_{rot} \approx 0.3$ d^{-1} which is at the low-frequency end of the SPB range. Therefore if a SPB frequency peak is mistaken for rotation, it most probably will be at a higher frequency. This will result in a ν_e larger than $\nu\sin i$ and will thus appear to confirm rotational modulation.

A single low frequency or a low frequency and its harmonic could possibly arise from SPB pulsation simply by coincidence. There is no known mechanism which preferentially selects just a single mode or a mode and its harmonic. Unless evidence for such a selection mechanism is found, it is difficult to accept SPB as a possible explanation for more than a few stars. In any case, pulsation can only occur if the star is within the instability strip. While the SPB instability strip may be extended to cooler stars by the effect of rotation, this explanation will ultimately fail for sufficiently cool stars. There are plenty of hot A stars which show a single low frequency or low frequency and harmonic well outside the SPB

Table 2. References to the effective temperatures in Table 1 andTable3.

Ref	Reference	Method
1	Pecaut & Mamajek (2013)	Spectral type
2	Urbaneja et al. (2017)	Spectroscopy
3	Gianninas, Bergeron & Ruiz (2011)	Spectroscopy
4	Paunzen, Schnell & Maitzen (2005)	Narrow-band photometry
5	Wright et al. (2003)	Spectral type
6	Balona (1994)	Strömgren
7	Chandler, McDonald & Kane (2016)	SED fitting
8	Gullikson, Kraus & Dodson-Robinson (2016)	Spectroscopy
9	Sánchez-Blázquez et al. (2006)	Spectroscopy
10	McDonald, Zijlstra & Watson (2017)	SED fitting
11	Geier et al. (2017)	Stectral type/SED
12	Oey & Massey (1995)	Sp.Type and UBV
13	Paunzen et al. (2013)	UBV/Geneva/Strömgren
14	David & Hillenbrand (2015)	Strömgren
15	De Cat & Aerts (2002)	Geneva
16	Silva & Napiwotzki (2011)	Strömgren
17	Zorec et al. (2009)	BCD method
18	Silaj & Landstreet (2014)	Geneva/Strömgren
19	Soubiran et al. (2016)	Spectral type
20	Massey (2002)	UBVR photometry
21	Niemczura et al. (2015)	Spectroscopy
22	Huber et al. (2016)	Spectroscopy
23	Balona et al. (2011)	Spectroscopy
24	Tkachenko et al. (2013)	Spectroscopy
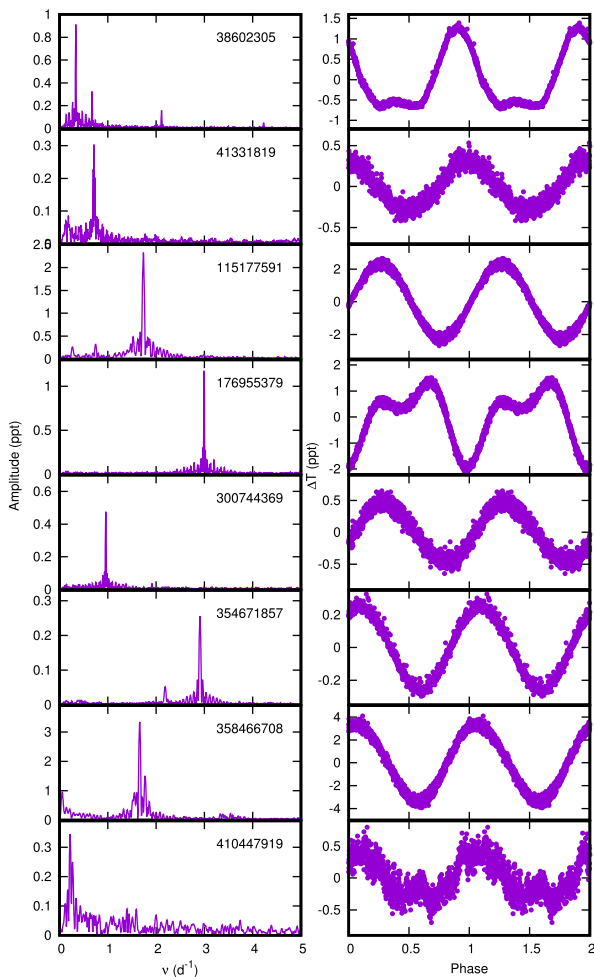
Figure 1. Examples of the periodograms (left-hand panels) and phased *TESS* light curves (right-hand panels) of a presumed rotational variables.

instability strip, no matter how much it can reasonably be extended. These cannot be due to SPB pulsation. It is thus reasonable to assume that a single peak or a peak and its harmonic, for which the evidence indicates rotational modulation in A stars, is also a result of rotational modulation in the B stars.

It is also possible that low frequencies may be a result of binarity or Doppler beaming. Considering the fact that most of the observed frequencies are around $1\,d^{-1}$, it follows that the components must be rather close to each other. Under these conditions we may expect to see eclipses or partial eclipses in most of the stars. It is for this reason that we tend to assign a classification of EB or EA (rather than ROT) to stars with amplitudes in excess of a few parts per thousand. It turns out that the large number of B stars classified as ROT all have small amplitudes (typically around 150 ppt). The binarity explanation therefore requires that all these stars have grazing eclipses, which is very unlikely.

For the reasons discussed above, we are confident that an ROT classification does indeed have a high probability of being due to rotational modulation, but do not exclude some contamination from pulsation and binarity. Our aim is not to prove that the ROT stars are due to rotational modulation, but merely to show that rotational modulation is not excluded.

The frequencies listed as ν_{rot} in Tables 1 and 3 are all highly significant according to the false alarm probability (Scargle 1982). Probabilities that the specified frequency is due to noise are always less than 10^{-6} and the ratio of the peak amplitude to background noise level is always greater than 10. The typical peak amplitude is around 135 ppm.

As already mentioned, one test for rotational modulation is to compare the equatorial rotational velocity, v_e, obtained from ν_{rot} and the stellar radius, with $v\sin i$. For this purpose, values of $v\sin i$ in Tables 1 and 3 were obtained from the catalogue of Glebocki & Gnacinski (2005). A few more recent values were found using SIMBAD. Fig. 3 shows $v\sin i$ as a function of v_e for the *TESS* main-sequence stars identified as ROT (solid circles) or SXARI (open circles) in Tables 1 and 3. As expected, most stars fall below the $\sin i = 1$ line. If the variation is not related to rotation, one would have expected both sides of the $\sin i = 1$ line to be populated.

The typical error in $v\sin i$ for B stars can be estimated from the catalogue of Glebocki & Gnacinski (2005). The error increases with $v\sin i$ and ranges between 0 and $60\,km\,s^{-1}$. A representative value of $\sigma_{v\sin i} = 30\,km\,s^{-1}$ is reasonable. From the error in $\log L/L_\odot$ and T_{eff} it is easy to calculate the error in v_e. This error depends almost entirely on the error in T_{eff}. The contribution from the luminosity error is small while the contribution from the error in ν_{rot} is entirely negligible. The typical value for the error in the derived equatorial rotational velocity is $\sigma_{v_e} \approx 40\,km\,s^{-1}$. These error bars are shown in Fig. 3.

The distribution of points in Fig. 3 is roughly what one would expect for rotational modulation. Most of the stars would be seen equator-on and hence most of the points will be near the $\sin i = 1$ line. Stars which are nearly pole-on would not show rotational modulation, which is consistent with the lack of stars at the bottom right corner of the figure.

An estimate for the angle of inclination of a particular star can be found by dividing $v\sin i$ by v_e. The error in the resulting value of $\sin i$ clearly increases as v_e approaches zero because $\sin i$ is the ratio of two small numbers and even a small error in $v\sin i$ and/or v_e will lead to a large error in $\sin i$. Only rapidly rotating stars are useful in estimating $\sin i$. As v_e approaches zero, the true range of $v\sin i$ also tends to zero and an increasing precision in $v\sin i$ is required to prevent it from exceeding v_e due to measurement errors. Since

Table 3. Additional rotational variables identified from the light curves of the *Kepler* and *K2* missions.

KIC/EPIC	Name	Var. type	V mag	ν_{rot} (d^{-1})	A_{rot} (ppm)	S/N	N_H	v_e (km s^{-1})	$v\sin i$ (km s^{-1})	T_{eff} (K)	Ref	$\log \frac{L}{L_\odot}$	Sp. type
EPIC 210788932	HD 23016	ROT	5.690	1.802	2743	39	0	351	260	11 463	6	2.36	B8Ve? (Be)
EPIC 211116936	HD 23324	SPB + ROT	5.640	1.543	161	19	1	252	206	12 218	6	2.32	B8:IV/V
EPIC 211028385	HD 23753	ROT	5.450	1.808	57	18	1	308	292	11 899	6	2.31	B8IV/V
EPIC 211054599	HD 23964	SXARI (UV)	6.740	0.633	470	26	1	77	21	10 190	6	1.75	B9.5VspSiSrCr
EPIC 210964459	HD 26571	SXARI (ACV:)	6.120	0.063	8910	40	0	22	22	11 430	6	2.85	B9IIIp:(Si)
EPIC 202061205	HD 253049	ROT	9.620	0.294	1714	23	1	90	184	22 570	1	3.93	B3III
EPIC 211311439	HD 74521	SXARI (ACV)	5.660	0.144	3938	10	0	29	18	10 615	6	2.26	B9pSiCr
EPIC 201232619	HD 97991	ROT	7.410	0.496	128	17	1	323	137	9956	6	3.16	B2/3V
EPIC 204760247	HD 142883	ROT	5.841	1.103	2562	18	0	254	19	9648	6	2.21	B3V
EPIC 204134887	HD 142884	SXARI (ACV)	6.777	1.245	5815	35	2	200	138	9979	6	1.95	kB8hB4HeB9V Si4200
EPIC 204348206	HD 143600	ROT (RS:)	7.330	3.922	205	33	3	452	265	9087	6	1.50	B9Vann
EPIC 204095429	HD 144844	SXARI	5.880	0.116	1002	36	1	25	98	9362	6	2.11	B9MnPGa
EPIC 204964091	HD 147010	SXARI (ACV)	7.400	0.255	12814	42	1	25	25	9092	6	1.38	B9SiCrSr∗
EPIC 205417334	HD 148860	ROT	8.040	0.920	152	21	1	177	257	9566	6	2.03	B9.5V
KIC 8351193	HD 177152	ROT	7.570	1.757	2	10	1	168	180	10 500	21	1.59	A0VkB8mB7 λ Boo
EPIC 217692814	HD 177015	ROT	7.800	1.139	50	13	1	448	202	10 567	22	2.83	B5V(e) (Be)
KIC 8087269	ILF1 + 43 30	ROT	11.710	1.610	1608	93	3	268	271	14 500	23	2.63	B5
KIC 9278405	ILF1 + 45 284	SPB/ROT	10.160	1.805	4	10	1	194	110	11 710	1	1.79	B9
KIC 4056136	BD + 38 3580	ROT	9.550	2.370	10	39	1	351	227	10 500	21	1.97	B9IV-Vnn
KIC 9468611		ROT	13.144	2.193	18	15	1	290	263	11 710	1	1.98	B9IV
KIC 6128830	BD + 41 3394	SXARI	9.190	0.206	1526	98	1	56	15	12 600	23	2.82	B6pHgMn
KIC 7974841	HD 187139	ROT	8.160	0.255	68	23	2	22	33	10 650	24	1.55	B8V
KIC 5477601		ROT	12.793	0.192	374	29	1	25	88	11 710	1	2.12	B9V
KIC 5130305	HD 226700	ROT	10.210	2.151	11	15	2	330	155	10 670	23	2.03	B9
KIC 8324268	HD 189160	SXARI(ACV:)	7.900	0.498	11 890	21	2	72	31	11 710	1	2.09	B9pSiCr
KIC 8389948	HD 189159	ROT	9.140	0.994	12	20	2	158	142	10 240	23	1.99	B9.5IV-V
KIC 5479821	HD 226795	ROT	9.890	0.588	13 586	25	2	119	85	14 810	23	2.84	B8
EPIC 206326769	HD 211838	SXARI	5.346	0.893	105	27	1	314	66	13 520	1	3.16	B8IIIp:(MnHg?)
EPIC 206097719	HD 213781	SXARI	9.000	0.181	456	24	0	62	34	15 330	1	3.36	B7Si

the error in $v\sin i$ is roughly the same over the whole range of v_e, it is inevitable that an increasing number of stars will lie above the $\sin i = 1$ line as v_e tends to zero.

Several stars lie above the $\sin i = 1$ line, including three SXARI stars for which rotational modulation is universally accepted as the cause of the light variation. TIC 270070443 is only slightly discrepant and a small change in $v\sin i$ or v_e will bring it below the $v\sin i = 1$ line. The $v\sin i$ values of TIC 280051467 range from 36–64 km s^{-1} and adopting the smaller value will remove the discrepancy. The same is true for the most discrepant SXARI star, TIC 204095429 with $v\sin i$ in the range 18–98 km s^{-1}.

There is, of course, nothing unphysical about stars lying above the $v\sin i = 1$ line. The location of a star in this diagram depends on two quantities which are both subject to error. A star lying above the line by more than three standard deviations is probably a result of mis-classification. Stars that do lie above the line may simply be a result of an error in $v\sin i$ and/or v_e. The error in v_e, for example, is sensitive to the error in T_{eff}. The interpretation of $v\sin i > 1$ in terms of the angle of inclination is that the star may be mis-classified as ROT or that the errors are too large for i to be measured, but that the inclination is probably nearly equator-on.

The most discrepant ROT star is TIC 355477670 with $v\sin i = 123$ km s^{-1} (Zorec & Royer 2012), $v_e = 37$ km s^{-1}. The estimated v_e is three times smaller than $v\sin i$. This star has the lowest amplitude (21 ppm) among the *TESS* stars, though the periodogram peak at 0.272 d^{-1} is prominent. *KELT* ground-based photometry gives a rotation period $P_{rot} = 27.15180$ d (Oelkers et al. 2018), which would make the discrepancy still larger. No evidence of such a period is found in the *TESS* data. Perhaps the observed periodicity is of a binary nature.

TIC 259862349 with $v\sin i = 96$ km s^{-1} and $v_e = 53$ km s^{-1} appears to be surrounded by a debris-disc (Welsh & Montgomery 2018). This is an another low-amplitude star (51 ppm) with a strange light curve. There is sudden doubling in the light amplitude variation which looks to be of instrumental origin. Although the periodogram peak is sharp, it is surrounded by noise which is likely related to the sudden change in the appearance of the light curve.

EPIC 202061205 is a variable of unknown type with a period of 3.414701 d (Watson, Henden & Price 2006), which is the same as in Table 3. The variability could possibly be a binarity effect considering that the amplitude is fairly large.

EPIC 205417334 has a period of 1.0877 d according to Rebull et al. (2018), the same as in Table 3, but no variability classification is given. Perhaps this is another binary.

It should be noted that the ROT classification was made with no prior knowledge of the literature on these stars. However, one star (EPIC 202909059) was removed after it was found to be a spectroscopic binary (it was the most discrepant point in the $v\sin i/v_e$ diagram). Thus there is no reason to suspect a bias regarding the allocation of the ROT class. Only four or five ROT stars are found to be somewhat discrepant which suggests that there are probably not many mis-classifications.

8 NOTES ON SOME ROT STARS

Stars which lie below the $\sin i = 1$ line but that are of interest are discussed below.

TIC 38602305 (HD 27657) is an optical double with a separation of 4 arcsec and a magnitude difference $\Delta V = 1.6$ mag with spectral
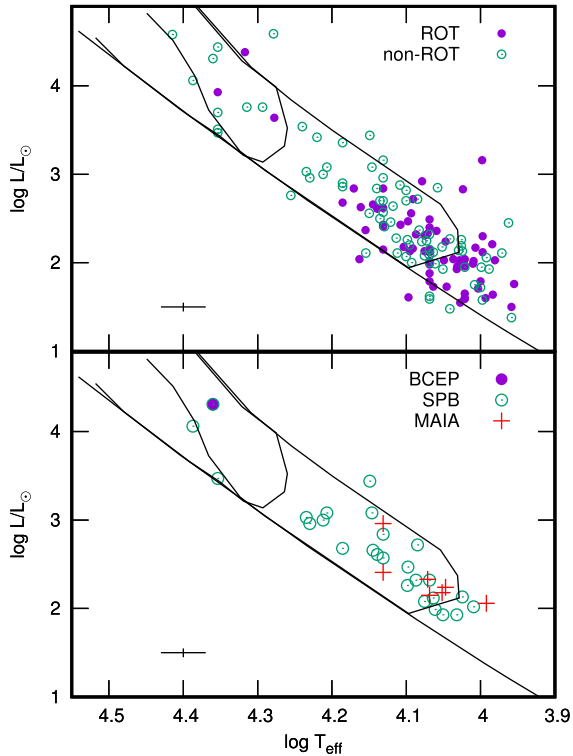
Figure 2. The theoretical H–R diagram for *TESS, Kepler,* and *K2* main-sequence stars. The top panel shows stars identified as possible rotational variables (filled circles). The open circles are other main-sequence stars (including the SXARI rotational variables). In the bottom panel pulsating variable stars in the *TESS* field are shown. The filled circle is the only BCEP star in the sample, HN Aqr. The open circles are stars classified as SPB variables. The crosses are MAIA stars. The solid line is the zero-age main sequence from solar-abundance models by Bertelli et al. (2008). The dashed and dotted areas are the theoretical BCEP and SPB instability regions from Miglio, Montalbán & Dupret (2007), respectively. The cross at the bottom shows the typical 1σ error bars.
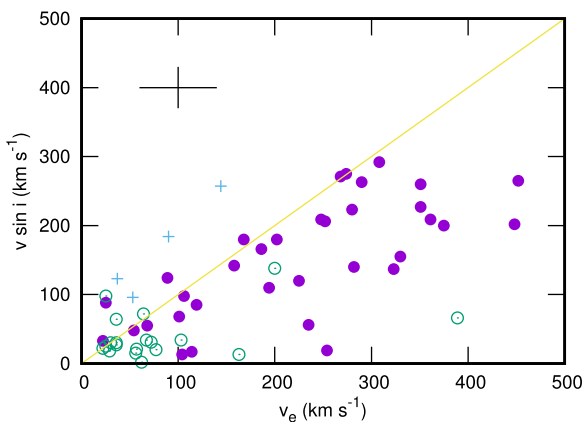
Figure 3. The projected rotational velocity, $v\sin i$, as a function of equatorial rotational velocity, v_e, for stars in the *TESS, Kepler,* and *K2* fields (filled circles). The open circles are SXARI stars which are rotational variables due to chemical abundance variations across the surface. The small crosses are discrepant stars discussed in the text. The straight line has unit slope, corresponding to $\sin i = 1$. The cross at the top left is the approximate 1σ error bars.

types B9III and B9V. A period of 27.15 d was reported by Oelkers et al. (2018) from *KELT* ground-based photometry. The *TESS* periodogram shows a peak with period 2.976 d and three of its harmonics (Fig. 1).

TIC 47296054 (HD 214748) is a classical Be star. Three harmonics of the fundamental at $0.836\,d^{-1}$ are clearly visible. The star seems to be a typical ROT variable. In addition, there is an anomalous peak at $0.432\,d^{-1}$ which is not part of the harmonic sequence. Thus a SPB + ROT classification was assigned.

TIC 139468902 (HD 213155) has a rotation period of 5.97 d from *KELT* photometry (Oelkers et al. 2018). The *TESS* data, on the other hand, has a fundamental period of 0.455 d with the first harmonic having a similar amplitude. No other significant frequencies seem to be present.

TIC 150357404 (HD 45796) has a rotation period of 2.78 d from *KELT* photometry (Oelkers et al. 2018). The *TESS* data gives $P_{\rm rot} =$ 1.56 d. The periodogram shows two weak sidelobes surrounding the central peak, hence the SPB + ROT? classification. The uncertainty is that perhaps the main peak is a pulsation mode and not due to rotation.

TIC 152283270 (HD 208433). This is a visual double separated by 0.6 arcsec with $\Delta V = 2.26$ mag. The periodogram shows a single peak at $0.434\,d^{-1}$ assumed to be rotation, but the light curve also shows a single clear eclipse with a duration of about 0.6 d and a depth of about 1 millimag. Hence the ROT? + EA classification. The uncertainty is due to the relatively low S/N of the supposedly rotation peak and the absence of harmonics.

TIC 238194921 (HD 24579). Apart from the peak at $\nu_{\rm rot} =$ $0.727\,d^{-1}$ and its harmonic, the are two additional peaks, the one at $1.812\,d^{-1}$ having the largest amplitude (190 ppm). The other peak is close to $\nu_{\rm rot}$ and with similar amplitude. These additional peaks indicate that this may be an SPB star. Hence the classification SPB + ROT.

TIC 262815962 (HD 218976) is a visual double with separation of 1.6 arcsec and $\Delta V = 3.91$ mag. A rotation period of 27.15 d is reported by Oelkers et al. (2018) from *KELT* data. The *TESS* data give $P_{\rm rot} = 2.71$ d.

TIC 271503441 (HD 2884) is a visual double with separation of 2.5 arcsec and $\Delta V = 9.1$ mag. In fact, there are another five associated, more widely separated, stars. The brightest star, β^1 Tuc, does not seem to be a spectroscopic binary (Chini et al. 2012). The *TESS* data show a peak at $3.056\,d^{-1}$ and its harmonic and nothing else of significance.

TIC 271971626 (HD 62153) is a visual double separated by 1.9 arcsec and of equal brightness and spectral types. The main periodogram peak at $0.215\,d^{-1}$ is assumed to be due to rotation. There is also a peak of lower amplitude ($A = 30$ ppm) at $5.820\,d^{-1}$ and its first harmonic ($A = 13$ ppm). The high frequency must be a pulsation, so we have assigned the MAIA class as the star lies between the red edge of the β Cep variables and the blue edge of the δ Sct stars.

TIC 277103567 (HD 37935) is a classical Be star. The periodogram shows a very simple series of peaks with fundamental at $1.496\,d^{-1}$ and up to three harmonics. The first harmonic has the highest amplitude. This seems to be a typical ROT variable.

TIC 279430029 (HD 53048) is another classical Be star. The periodogram is very simple and consists of just two peaks: the fundamental at $1.784\,d^{-1}$ and the first harmonic which has twice the amplitude. This is a ROT variable.

KIC 293268667 (HD 47478). The periodogram shows multiple peaks in the range $2.8–3.9\,d^{-1}$ and also at $6.6–7.1\,d^{-1}$. The multiple peaks suggest an SPB star. The harmonic of the main peak at

3.390 d^{-1} is visible with the same amplitude as the fundamental. Hence the classification SPB + ROT.

TIC 300010961 (HD 55478). The periodogram shows a strong peak at 0.683 d^{-1} with three visible harmonics. In addition there are multiple peaks in the range 17–45 d^{-1}. Because of its location in the H–R diagram we classify it as a MAIA variable. The star is a visual double (2.2 arcsec, $\Delta V = 2.9$ mag).

TIC 300329728 (HD 59426). The fundamental peak has a large amplitude. For this reason it might be considered an ellipsoidal (ELL) variable, but could also be ROT. The first harmonic is prominent.

TIC 308537791 (HD 67277). The fundamental at 0.527 d^{-1} and its first harmonic is present. In addition, a peak at 7.397 d^{-1} and at least three of its harmonics can be seen. The high frequency suggests pulsation, so it has been given the classification ROT + MAIA.

TIC 355653322 (HD 224686) is a classical Be star. The periodogram shows only a weak peak at 1.266 d^{-1} and its first harmonic. Apart from this, no other significant peaks are present.

TIC 419065817 (HD 1256). The periodogram shows a peak at 1.474 d^{-1} and at least three harmonics. However, there is also an unrelated peak at 0.226 d^{-1}.

TIC 441182258 (HD 210934) has a weak peak in the periodogram at 1.274 d^{-1} and some unresolved structure around 0.5 d^{-1}. This is classified as SPB + ROT?

EPIC 211116936 (HD 23324) has a strong frequency peak consisting of two close components. The first harmonic of one of the components is present, from which we suggest a ROT classification, but other low-frequency peaks exist which indicate that it is also SPB. The star is a member of the Pleiades.

KIC 9278405 (ILF1 + 45 284) was classified as SPB by McNamara, Jackiewicz & McKeever (2012). The star has a strong peak with multiple close components and a weak first harmonic. It could be indeed classified as SPB, but differential rotation will also account for the structure in the main peak.

KIC 5479821 (HD 226795) has a single sharp peak and harmonic. McNamara et al. (2012) classified the star as either a binary or rotational variable with the period listed in Table 3.

9 FLARE STARS

Optical stellar flares are usually associated with active M dwarfs which can dramatically increase in brightness over a broad wavelength range from X-rays to radio waves for anywhere from a few minutes to a few hours. The rapid rise in brightness is followed by a slow decay with a time-scale from minutes to hours. The largest change in brightness occurs at short wavelengths: a rise of one magnitude in the *V* band is typically accompanied by a rise of five magnitudes in the *U* band. The amplitudes are much lower in the very wide band used in the *TESS* and *Kepler* observations.

Flares in the Sun are caused by energy released by the reconnection of magnetic field lines in the outer atmosphere. The energies released in solar flares are in the range 10^{29}–10^{32} erg. Flares in active M dwarfs are typically 10–1000 times more energetic than solar flares. Although we have a very limited understanding of stellar flares, it is thought that the underlying mechanism is essentially the same as in the Sun.

The *Kepler* mission has resulted in the discovery of 'super-flares' in solar-type stars with energies in the range 10^{33}–10^{36} erg (Maehara et al. 2012). More surprisingly, flaring was found in about 2.5 per cent of A stars (Balona 2012, 2013, 2015). Spec-

troscopic observations of the A-type flare stars suggest significant contamination by field stars in the *Kepler* aperture and that many of the stars are spectroscopic binaries (Pedersen et al. 2017). The possibility that the flares originate in a companion certainly cannot be discounted. However, it should be noted that the flares associated with A stars are 100–1000 times more energetic than those in typical M or K dwarfs (Balona 2015), suggesting that they may originate in the A star and not on a late-type companion.

In the course of inspection of the *TESS* light curves, we came across three stars which appear to flare (Fig. 4). TIC 92136299 is a normal B9.5IV star with clear periodic variations suggestive of rotational modulation. The periodogram shows a main peak at 2.251 d^{-1} and its first harmonic. In addition, there is a third peak at 2.642 d^{-1} which could be interpreted as a second 'spot' in a differentially rotating star. Two flare-like events can be seen which have the typical sharp rise and slow decay of a stellar flare. According to Chini et al. (2012), the star is not a spectroscopic binary.

TIC 92136299 (ω^2 Aqr A) has a close companion, (ω^2 Aqr B) with spectral type A5IVpec with the H&K CaII lines in emission (Gahm, Ahlin & Lindroos 1983). The stars are separated by 5 arcsec and magnitude difference of 6 mag. The pair is an X-ray source (Makarov 2003).

A flare is also found in TIC 118327563 which is a subdwarf B star. Bagnulo et al. (2015) was unable to detect a significant magnetic field. The rapid light variation of 4.372 d^{-1} is clearly seen in the light curve. The periodogram shows two closely spaced peaks at 4.372 and 4.203 d^{-1} and their first harmonics.

The flare on TIC 224244458 (β Scl) is very interesting as this is a HgMn star. The HgMn stars are chemically peculiar stars containing an excess of P, Mn, Ga, Sr, Yt, Zr, Pt, and Hg. They lack a strong dipole magnetic field and are slow rotators. For β Scl, Bychkov, Bychkova & Madej (2009) quotes a (null) magnetic field measurement of 61 ± 36 G. Chini et al. (2012) found that the star is not a spectroscopic binary.

We can calculate the approximate flare energy from the area occupied by the flare in the light curve and the stellar luminosity. These turn out to be approximately 10^{36} erg for TIC 92136299 and TIC 224244458 and 10^{35} erg for TIC 118327563, which are all considerably larger than the most energetic flares in typical K or M dwarfs, but similar to the flare energies in A stars. This does not prove that the flares originate on B stars, but is an indication that this might be the case.

10 OTHER STARS OF INTEREST

The only β Cep star in the sample is TIC 69925250 (HN Aqr). *TESS* observations of the star are discussed by Handler et al. (2019).

There are 25 stars classified as SPB variables in the *TESS* data. The classification is based on the presence of multiple low-frequency peaks. In some stars one may interpret a strong peak and its harmonic as possibly due to rotation. These have been designated SPB + ROT variables and are treated as both SPB and rotational variables.

The 12 stars considered to be classical Be stars are designated in the last column of Table 1 by '(Be)'. Many of them display broad multiple peaks considered to be a result of nonradial pulsation or variable circumstellar obscuration. These are classified as BE variables, in accordance with the GVCS definition. In addition to the broad peaks, TIC 270219259 also shows a strong, sharp peak at 7.445 d^{-1}. The star is too cool for a BCEP, so we have classified it as
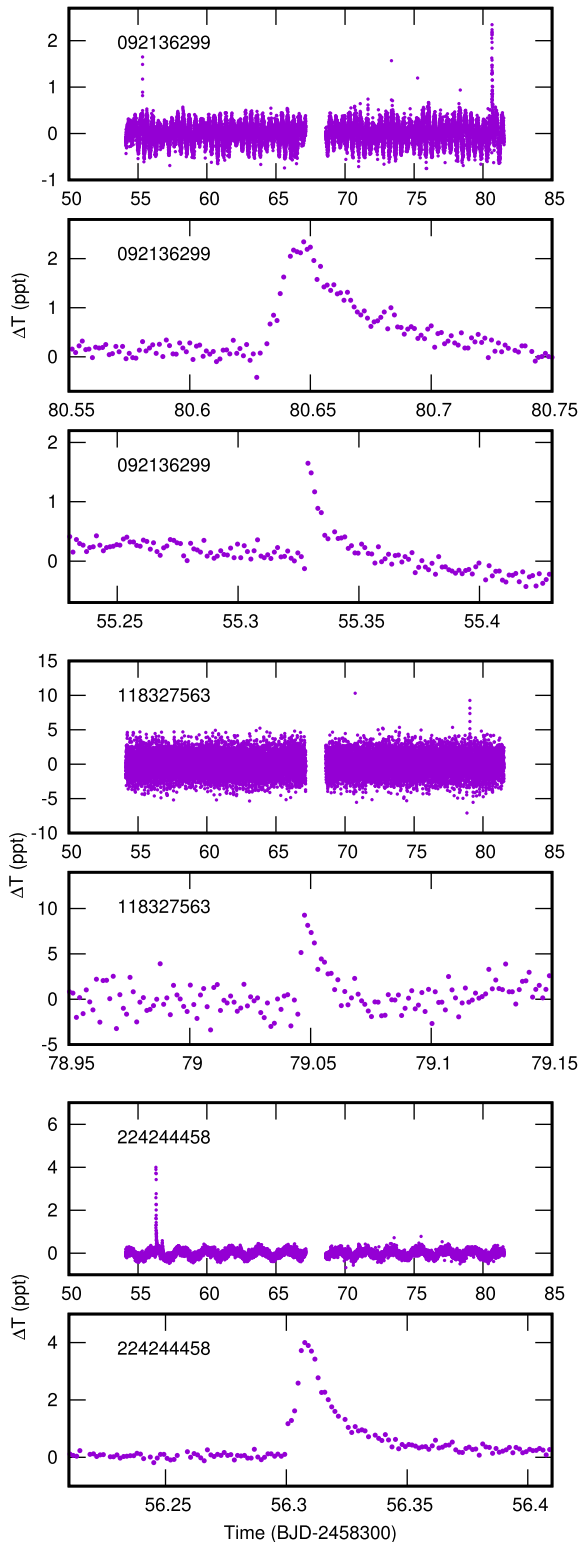
Figure 4. Light curves of three stars (TIC numbers given) which appear to show one or more flares. The units for the light variation are parts per thousand (ppt).

BE/MAIA. TIC 308748912 does not have any significant peaks with frequencies higher than $0.5\,d^{-1}$ and with amplitudes above 10 ppm. Four classical Be stars have already been discussed in Section 8 and appear to be normal rotational variables. Two additional classical

Be stars, EPIC 210788932, and EPIC 217692814 also seem to be typical ROT variables.

Of the seven stars classified as MAIA variables, three have $v\sin i$ measurements. This brings to 16 the number of suspected MAIA stars with known $v\sin i$, for which the mean is $<v\sin i> = 111 \pm 23\,km\,s^{-1}$. This does not suggest that rapid rotation is an important factor, unlike the FaRPB stars.

TIC 169285097 (J2344-3427) is a known subdwarf pulsating B star (Holdsworth et al. 2017). The *TESS* data show that it pulsates in both long- and short periods (hybrid V361 Hya/V1093 Her star). There are dozens of peaks in the range $8 < \nu < 60\,d^{-1}$, but also a few peaks in the range $220 < \nu < 250\,d^{-1}$. The other sdB stars and the white dwarf TIC 31674330 appear to be constant.

Another class of interest are rotational variables with detected magnetic fields in the first *TESS* data release. These are being investigated by David-Uraz et al. (in preparation).

11 CONCLUSIONS

For the last half-century the view that stars with radiative envelopes cannot sustain a magnetic field and are therefore devoid of starspots has been generally assumed. Suspicions that this was not the case have occasionally arisen, particularly from inspection of good ground-based photometric time series of δ Sct and β Cep stars, where the presence of significant low frequencies has sometimes been noted. However, owing to the fact that the rotational periods of A and B stars are close to one day, it is very difficult to detect low-amplitude rotational modulation of A and B stars in ground-based photometry from a single site.

With the advent of precise time-series photometry from space it has become apparent that rotational modulation is very likely present in about half the A stars in the *Kepler* field (Balona 2013, 2017). This is demonstrated by the fact that the photometric period distribution closely matches the expected distribution from spectroscopic $v\sin i$ measurements (Balona 2013). Furthermore, the expected relation between the equatorial rotational velocity, v_e, estimated from the photometric period and $v\sin i$ is also present (Balona 2017).

There are very few B stars in the *Kepler* and *K2* fields (most of them are late B stars), too few to calculate the v_e distribution and compare it with the v_e distribution expected from spectroscopic $v\sin i$ measurements from field stars in the same temperature range. Balona (2016) was able to identify presumed rotational modulation in many B stars observed with the *K2* mission, but for the most part $v\sin i$ measurements were not available to test the relationship with v_e.

In this paper we examined the light curves of 160 B stars observed by *TESS* and classified them according to variability type. It appears that a large fraction of these stars may be rotational variables without any known chemical peculiarity. Balona (2016) had already arrived at the same conclusion from a sample of *K2* B stars.

Using *Gaia* parallaxes, the luminosities of these main-sequence stars were estimated, from which the radii can be found. From the radii and the photometric periods, the equatorial rotational velocities can be determined. The expected relationship between projected rotational velocity and the equatorial rotational velocity is found, confirming that the photometric periods are consistent with rotation.

Out of the 112 main-sequence B stars observed by *TESS*, 45 were classified as rotational variables or possible rotational variables. This fraction (about 40 per cent) is similar to the fraction of rotational variables found among the A stars (Balona 2013) and a

confirmation of a similar result from B stars in the *K2* field (Balona 2016). Rotational variability appears to be the most common type of light variation among A and B main-sequence stars. None of these variables are known to be chemically peculiar.

This result calls into question current models of the outer layer of stars with radiative envelopes. Cantiello et al. (2009) and Cantiello & Braithwaite (2011) have suggested that magnetic fields produced in subsurface convection zones could appear on the surface. Thus localized magnetic fields could be widespread in those early-type stars with subsurface convection. Magnetic spots of size comparable to the local pressure scale height are predicted to manifest themselves as hot, bright spots (Cantiello & Braithwaite 2011). Recent observations from space indicate that bright spots may have been detected in some O stars (Ramiaramanantsoa et al. 2014; David-Uraz et al. 2017; Ramiaramanantsoa et al. 2018). It is also possible that differential rotation in the A and B stars may be sufficient to create a local magnetic field via dynamo action (Spruit 1999, 2002; Maeder & Meynet 2004). Whether or not any of these ideas relates to rotational modulation as observed in A and B stars requires further work.

ACKNOWLEDGEMENTS

REFERENCES

Bagnulo S., Fossati L., Landstreet J. D., Izzo C., 2015, A&A, 583, A115
Balona L. A. et al., 2011, MNRAS, 413, 2403
Balona L. A. et al., 2016, MNRAS, 460, 1318
Balona L. A., 1994, MNRAS, 268, 119
Balona L. A., 2012, MNRAS, 423, 3420
Balona L. A., 2013, MNRAS, 431, 2240
Balona L. A., 2015, MNRAS, 447, 2714
Balona L. A., 2016, MNRAS, 457, 3724
Balona L. A., 2017, MNRAS, 467, 1830
Balona L. A., 2018, MNRAS, 479, 183
Balona L. A., Baran A. S., Daszyńska-Daszkiewicz J., De Cat P., 2015, MNRAS, 451, 1445
Bertelli G., Girardi L., Marigo P., Nasi E., 2008, A&A, 484, 815
Brown T. M., Latham D. W., Everett M. E., Esquerdo G. A., 2011, AJ, 142, 112
Bychkov V. D., Bychkova L. V., Madej J., 2009, MNRAS, 394, 1338
Cantiello M. et al., 2009, A&A, 499, 279
Cantiello M., Braithwaite J., 2011, A&A, 534, A140
Chandler C. O., McDonald I., Kane S. R., 2016, AJ, 151, 59
Charbonneau P., 2014, ARA&A, 52, 251
Chini R., Hoffmeister V. H., Nasseri A., Stahl O., Zinnecker H., 2012, MNRAS, 424, 1925
Chowdhury S., Joshi S., Engelbrecht C. A., De Cat P., Joshi Y. C., Paul K. T., 2018, Ap&SS, 363, 260
Crawford D. L., 1978, AJ, 83, 48
David-Uraz A., Owocki S. P., Wade G. A., Sundqvist J. O., Kee N. D., 2017, MNRAS, 470, 3672
David T. J., Hillenbrand L. A., 2015, ApJ, 804, 146
De Cat P., Aerts C., 2002, A&A, 393, 965
Dziembowski W. A., Moskalik P., Pamyatnykh A. A., 1993, MNRAS, 265, 588
Gahm G. F., Ahlin P., Lindroos K. P., 1983, A&AS, 51, 143
Gaia Collaboration, 2016, A&A, 595, A1
Gaia Collaboration, 2018, A&A, 616, A1
Geier S., Østensen R. H., Nemeth P., Gentile Fusillo N. P., Gänsicke B. T., Telting J. H., Green E. M., Schaffenroth J., 2017, A&A, 600, A50
Gianninas A., Bergeron P., Ruiz M. T., 2011, ApJ, 743, 138
Glebocki R., Gnacinski P., 2005, VizieR Online Data Catalog, 3244
Gontcharov G. A., 2017, Astron. Lett., 43, 472
Gullikson K., Kraus A., Dodson-Robinson S., 2016, AJ, 152, 40
Hall D. S., 1972, PASP, 84, 323
Handler G. et al., 2019, ApJ, submitted
Holdsworth D. L., Østensen R. H., Smalley B., Telting J. H., 2017, MNRAS, 466, 5020
Huber D. et al., 2016, ApJS, 224, 2
Jenkins J. M. et al., 2016, in Proc. SPIE Conf. Ser. Vol. 9913, Software and Cyberinfrastructure for Astronomy IV. SPIE, Bellingham, p. 99133E
Kron G. E., 1947, PASP, 59, 261
Maeder A., Meynet G., 2004, A&A, 422, 225
Maehara H. et al., 2012, Nature, 485, 478
Makarov V. V., 2003, AJ, 126, 1996
Massey P., 2002, ApJS, 141, 81
McDonald I., Zijlstra A. A., Watson R. A., 2017, MNRAS, 471, 770
McNamara B. J., Jackiewicz J., McKeever J., 2012, AJ, 143, 101
McQuillan A., Mazeh T., Aigrain S., 2013, ApJ, 775, L11
McQuillan A., Mazeh T., Aigrain S., 2014, ApJS, 211, 24
Michaud G., 1970, ApJ, 160, 641
Miglio A., Montalbán J., Dupret M., 2007, Commun. Asteroseismol., 151, 48
Mowlavi N., Saesen S., Semaan T., Eggenberger P., Barblan F., Eyer L., Ekström S., Georgy C., 2016, A&A, 595, L1
Nielsen M. B., Gizon L., Schunker H., Karoff C., 2013, A&A, 557, L10
Niemczura E. et al., 2015, MNRAS, 450, 2764
Oelkers R. J. et al., 2018, AJ, 155, 39
Oey M. S., Massey P., 1995, ApJ, 452, 210
Paunzen E., Schnell A., Maitzen H. M., 2005, A&A, 444, 941
Paunzen E., Wraight K. T., Fossati L., Netopil M., White G. J., Bewsher D., 2013, MNRAS, 429, 119
Pecaut M. J., Mamajek E. E., 2013, ApJS, 208, 9
Pedersen M. G. et al., 2019, ApJ, submitted, 872, L9
Pedersen M. G., Antoci V., Korhonen H., White T. R., Jessen-Hansen J., Lehtinen J., Nikbakhsh S., Viuho J., 2017, MNRAS, 466, 3060
Ramiaramanantsoa T. et al., 2014, MNRAS, 441, 910
Ramiaramanantsoa T. et al., 2018, MNRAS, 473, 5532
Rebull L. M., Stauffer J. R., Cody A. M., Hillenbrand L. A., David T. J., Pinsonneault M., 2018, AJ, 155, 196

Reinhold T., Reiners A., Basri G., 2013, A&A, 560, A4

Ricker G. R. et al., 2015, J. Astron. Telesc. Instrum. Syst., 1, 014003

Samus N. N., Durlevich O. V. et al., 2009, VizieR Online Data Catalog, 1, 2025

Sánchez-Blázquez P. et al., 2006, MNRAS, 371, 703

Scargle J. D., 1982, ApJ, 263, 835

Silaj J., Landstreet J. D., 2014, A&A, 566, A132

Silva M. D. V., Napiwotzki R., 2011, MNRAS, 411, 2596

Soubiran C., Le Campion J.-F., Brouillet N., Chemin L., 2016, A&A, 591, A118

Spruit H. C., 1999, A&A, 349, 189

Spruit H. C., 2002, A&A, 381, 923

Stassun K. G. et al., 2018, AJ, 156, 102

Strassmeier K. G., 2009, A&AR, 17, 251

Tkachenko A., Lehmann H., Smalley B., Uytterhoeven K., 2013, MNRAS, 431, 3685

Urbaneja M. A., Kudritzki R.-P., Gieren W., Pietrzyński G., Bresolin F., Przybilla N., 2017, AJ, 154, 102

Watson C. L., Henden A. A., Price A., 2006, The International Variable Star Index (VSX). The Society for Astronomical Sciences. CA, U.S., p. 47

Welsh B. Y., Montgomery S. L., 2018, MNRAS, 474, 1515

Wenger M. et al., 2000, A&AS, 143, 9

Wright C. O., Egan M. P., Kraemer K. E., Price S. D., 2003, AJ, 125, 359

Zorec J., Royer F., 2012, A&A, 537, A120

Zorec J., Cidale L., Arias M. L., Frémat Y., Muratore M. F., Torres A. F., Martayan C., 2009, A&A, 501, 297

This paper has been typeset from a TEX/LATEX file prepared by the author.